Journal of Inorganic Biochemistry 264 (2025) 112793

Contents lists available at ScienceDirect

Journal of Inorganic Biochemistry

journal homepage: www.elsevier.com/locate/jinorgbio

Insight into uranyl binding by cyclic peptides from molecular dynamics and density functional theory

James A. Platts [a,*], Iogann Tolbatov [b,c]

[a] School of Chemistry, Cardiff University, Park Place, Cardiff CF10 3AT, UK
[b] Department of Chemical, Physical, Mathematical and Natural Sciences, University of Sassari, 07100 Sassari, Italy
[c] Department of Physics and Astronomy, University of Padova, Via F. Marzolo 8, 35131 Padova, Italy

ARTICLE INFO

Keywords:
Uranyl binding
Metal-binding peptide
Cationic dummy atom model
Molecular dynamics
Density functional theory

ABSTRACT

It is a challenging task to develop uranyl-chelating agents based on peptide chemistry. A recently developed cationic dummy atom model of uranyl in conjunction with the classical molecular dynamics simulation presents a helpful utility to study the chelation of uranyl by peptides with a low computational cost. In the present study, it was used to describe the chelation of uranyl by the cyclic decapeptide with 4 Glu residues cyc-GluArgGluProGlyGluTrpGluProGly and its derivatives containing two phosphorylated serines in place of two Glu, termed pS16, pS18, pS38, and pS68. The obtained structures were further studied by density functional theory (DFT) and subsequent density analysis. We show that a combination of steered molecular dynamics and simulated annealing, using standard forcefields for peptide with the cationic dummy atom model of uranyl, can quickly and reliably obtain binding modes of uranyl-peptide complexes. Classical molecular dynamics simulation in explicit water produces geometry very close to the DFT-optimized structure. The presence of uranyl completely changes the conformation of these cyclic peptides from unstructured to organised. The simulation of a peptide with two uranyl units explained why only the 1:1 ratio of peptide and chelated-uranyl is observed experimentally in most cases, by the insufficiency of the anionic residues for the chelation of two UO_2^{2+} units, but that pS16 can accommodate two such units.

1. Introduction

Despite its presence in mineral ores, soil, and water, uranium is not a natural element used by living organisms, and exposure gives rise to radiological and especially chemical toxicity [1]. Uranium in blood tends to bind to proteins, erythrocytes, and other biomolecules [2], causing harsh impacts on health, even though only up to 1.5 % of uranium is absorbed in organism [3]. This heavy metal mainly accumulates in bone and kidney, resulting in renal dysfunction and augmenting the probability of osteosarcoma [4,5]. Uranium occurs in various oxidation states, ranging from III to VI, the states IV and VI being the most ubiquitous in nature [6]. In physiological conditions, the uranyl cation $[U(VI)O_2]^{2+}$ is prevalent and constitutes a linear molecule with U(VI) in the centre, making possible coordination of 4–6 ligands in the equatorial plane perpendicular to the O-U-O axis. Being a hard Lewis acid, according to hard and soft acids and bases (HSAB) theory [7], uranyl exhibits high affinity toward hard oxygen donors. On the other hand, as a hard acid, it resembles the hard cation Ca^{2+}, this similitude explaining its ability to substitute Ca^{2+} in bones [8,9].

That is why it is a challenging task to develop uranyl-chelating agents since there is a necessity to create selectivity over Ca^{2+} cations that are present in high quantity in physiological milieu. At least a femtomolar affinity to uranyl is requisite to compete with the high level of solvated carbonate [10]. Various uranyl sequestering agents are based on the coordination of uranyl in sites rich with hard oxygen donors, such as phosphines, phosphates, phenolates and carboxylates [11,12]. The affinity toward uranyl was revealed in various proteins, including transferrin [13], albumin [14], calmodulin [15], and osteopontin (OPN) [16,17], the latter demonstrating an especially elevated affinity for uranyl [17,18]. Indeed, a recent investigation has disclosed an ability of human OPN to bind uranyl with high affinity [17]. Although the uranyl-binding sites in OPN were not established, there are a plethora of indirect experimental evidence of the major role of the polyphosphorylated residues, particularly serine, in the chelation of uranyl [16,19–21]. In a recent study, cyclic preorganized peptides, mimicking the highly phosphorylated binding sites of OPN, were designed and synthesized in such

* Corresponding author.
E-mail address: platts@cardiff.ac.uk (J.A. Platts).

https://doi.org/10.1016/j.jinorgbio.2024.112793
Received 5 August 2024; Received in revised form 19 November 2024; Accepted 27 November 2024
Available online 2 December 2024
0162-0134/© 2024 The Authors. Published by Elsevier Inc. This is an open access article under the CC BY license (http://creativecommons.org/licenses/by/4.0/).

a way that they incorporated two phosphoserines and two glutamic acids in the metal-binding motif [20]. These peptides revealed a high affinity for uranyl, thus corroborating the importance of phosphorylated residues in the cyclic peptide [20].

Computational chemistry studies yield significant results disclosing the chemistry of uranyl species. DFT was used to investigate the coordination of uranyl in water [22,23]. The reduction of uranyl, occurring in cytochrome *c7* in the bacteria *D. acetoxidans* and *G. sulfurreducens* [24], was also studied *via* DFT, corroborating experimental results and demonstrating the coordination of uranyl to carboxylates. The coordination of uranyl in super uranyl binding protein (SUP) [25], calmodulin [26], and apotransferrin [27] was analysed computationally, indicating the binding with aspartate, glutamate, and the phenolate of tyrosinate. However, the main drawback of DFT, its high computational cost, restricts its employment to only smaller, simplified models treated with implicit solvation.

On the other hand, molecular dynamics (MD), based on Newtonian mechanics applied to atoms, gives the possibility to investigate whole proteins. The choice of a classical force field is crucial in these simulations [28]. Although the earlier force fields correctly reproduced the uranium-water distances [29–31], the inclusion of polarizability in the potential augmented the computational burden. Another force field [32] yielded the correct hydration free energy of uranyl, however, permitting the spurious formation of hydrogen bonds between UO_2^{2+} oxygens and water. The effective pairwise potentials developed for actinyls AnO_2^{n+} ($n = 1, 2$) describing U—Am [33,34] also produced accurate hydration free energies, but overestimated An(VI)-oxygen distances. The difficulty of designing a force field to describe uranyl is one of the reasons of the rarity of its MD simulations. Recently, the geometry of super uranyl binding protein SUP was investigated *via* MD, studying the effect produced by uranyl on SUP [25,35]. MD simulations of calmodulin and ubiquitin revealed conformational consequences of the presence of uranyl [36,37].

Recently, a multisite cationic dummy atom (CDA) model of the uranyl cation, suitable for atomistic simulation of its interaction with water and biomolecules, was constructed [38]. The usage of this CDA model, designed as the UO_2^{2+} molecule with five rigidly fixed dummies located in the equatorial plane, each bearing a fraction of the charge and mass of the cation, allowed for the accurate reproduction of the geometry of model complexes with typical ligands and of the diffusion coefficient in water. Moreover, it permitted to obtain the correct structure of a uranyl-SUP adduct.

In the present study, we performed the molecular dynamics simulation of uranyl with a set of phosphorylated cyclodecapeptides pS16, pS18, pS38, and pS68 [20], along with the parent cyclic peptide with 4 Glu residues (cyc-GluArgGluProGlyGluTrpGluProGly) [11]. These cyclic preorganized peptides were synthesized in a recent study with an intention to mimic the highly phosphorylated binding sites of OPN [20,21]. Their design includes the incorporation of two phosphoserines and two glutamic acids in the metal-binding motif. These peptides revealed a high affinity for uranyl, evidencing the importance of the availability of the phosphorylated residues in the peptide loop. The objective of this paper is to obtain the mechanistic understanding of how these cyclopeptides chelate uranyl and also to test our CDA model of uranyl.

2. Methods

Cyclic peptides were built from sequence using the leap utility of AmberTools [39], with phosphorylated residues and bonds between N and C termini added as necessary. The resulting structures were minimised, then the cationic dummy atom model of uranyl [38] added in the vicinity of, but not specifically bound to, the peptide. Steered molecular dynamics, using a harmonic force constant of 10 kcal mol^{-1} $Å^{-1}$, was then used to push the centres of mass of uranyl and peptide Cα together. In some cases (*vide infra)* a further steered MD run and/or simulated annealing was used to search for lower energy coordination modes. These initial searches were performed using ff14SB forcefield [40] and GBSA implicit water model [41] (igb = 5) without any cutoff of electrostatic interactions.

Following steered MD searches, the resulting structures were solvated in a truncated octahedral box of TIP3P water [42] and neutralised by addition of appropriate number of Na^+ ions. This solvated structure was minimised and heated to 300 K in NPT ensemble over 2 ns, followed by production MD run of 100 ns in NPT ensemble, with 2 fs timestep enabled by restriction of bonds to hydrogen using SHAKE [43]. Analysis of the resulting trajectories used cpptraj [44] v6.18.1 from AmberTools, with clustering using k-means algorithm to generate 10 clusters. The same MD and clustering procedure was carried out for metal-free peptides to provide a reference. Radial distribution function, g(r), is used to measure the increased density of the specified atoms over the density of the bulk, to measure coordination number to different possible donor atoms. CD spectra were predicted using the PDBMD2CD server https://pdbmd2cd.cryst.bbk.ac.uk/ [45].

The most populated cluster was minimised in TIP3P water, before explicit water and ions being stripped out to leave the uranyl-peptide complex for DFT analysis. These used B3LYP-GD3BJ [46–48] with Stuttgart 1997 ECP on U [49,50] and 6–311++G** on remaining atoms [51,52] in PCM implicit model of water [53], in Gaussian16 Rev. B.01 [54]. Subsequent QTAIM analysis employed AIMAll v19.02.13 [55], concentrating on the electron density at the bond critical point (bcp), the point of minimum electron density along the relevant bond path, which is widely used as a proxy for bond strength.

3. Results and discussion

Initial steered MD typically resulted in an energy minimum involving three of the anticipated binding residues (Glu and/or pSer), but in one case (pS16) steered MD immediately docked uranyl to all four anionic side chains (Table 1). In the remaining cases, a second steered MD resulted in structures bound through four anionic residues, in agreement with experimental data [20]. For these cyclic decapeptides, conformational searching using self-guided Langevin dynamics was not able to leave the local energy minimum from first steered MD, in contrast to behaviour found for shorter, linear peptides in our previous work. This approach was therefore not pursued further (data not shown). Table 1 shows that there is no clear pattern in which residues bind uranyl on first approach, with both Glu and pSer left free. Pushing the fragments together results in large reduction in potential energy, in the region of *ca.* 600–700 kJ mol^{-1}. For all phosphorylated peptides, steered MD and simulated annealing resulted in effectively identical structures and minor differences in potential energy, but for the 4Glu peptide simulated

Table 1
Results of initial steered MD simulations. Rel E refers to energies relative to initial non-bonded complex, in kJ mol^{-1}.

	After SMD1	After SMD2	After Anneal
4Glu	Bound: E3, E6, E8 Free: E1 @ 8 Å Rel E − 623	Bound: E1, E3, E6, E8 Rel E − 628	Bound: E1, E3, E6, E8 Rel E − 711
pS16	Bound: pS1, E3, pS6, E8 Rel E − 661	N/A	Bound: pS1, E3, pS6, E8 Rel E − 664
pS18	Bound: pS1, E3, pS8 Free: E6 @ 9 Å Rel E − 590	Bound: all Rel E − 766	Bound: all Rel E − 674
pS38	Bound: E1, E6, pS8 Free: pS3 @ 10 Å Rel E − 640	Bound: E1, pS3, E6, pS8 Rel E − 749	Bound: all Rel E − 758
pS68	Bound: E1, E3, pS6 Free: pS8 @ 5 Å Rel E − 682	Bound: all Rel E − 732	Bound: all Rel E − 740

annealing gave a structure 84 kJ mol^{-1} lower than SMD, in which all four anionic side chains are bound to uranyl.

Explicit solvent MD runs starting from the endpoints highlighted in Table 1 are stable, as evidenced by plots of RMSD against time (Fig. S1). However, within that overall picture significant variation in coordination around uranyl is evident. In particular, variations in the coordinating atom(s) in the anionic residues are common, occurring in timescales of a few nanoseconds. This was observed mainly in Glu residues, for which κ2-chelation was rarely observed but switching between OE1 and OE2 regularly occurred. For pSer residues, a mixture of κ1 and κ2-coordination was observed, again with regular changes of specific atoms involved over timescales of around 10 ns, such that both pSer residues exhibit transient bidentate coordination despite starting points being monodentate. This is illustrated for one example (pS38) in Fig. 1. Peptide oxygen atoms make fleeting contribution to uranyl coordination: in most cases minimum U…O distances are around 2.5 Å, but these persist for just a few MD frames before anionic side chains return to dominate coordination.

Given these variations and the possibility of explicit water also contributing to coordination, radial distribution functions to possible ligand atoms are a more useful measure of interactions. RDF plots from a typical case are shown in Fig. 1, showing that all ligand peaks for the first shell lie within 2–3 Å, with further peaks for outer coordination shells. Integrated radial distribution functions characterise coordination modes over the length of each trajectory (Table S1). The 4Glu peptide has, on average, just less than 5.0 ligands from Glu residues, and a minor contribution (0.8) from explicit water. Changing two residues to pSer results in a striking change, with all backbone and solvent atoms excluded from the first shell. However, within the four phosphorylated peptides there exists significant variation in the balance between Glu and pSer: three peptides have approximately three pSer atoms bound to U, with two from Glu, but pS16 reverses this trend to have Glu dominate. Summing these values gives an estimate of the average coordination number around the equatorial plane: for 4Glu is slightly more than 5.5, whereas for all four phosphorylated peptides are almost exactly 5.0.

To probe these differences in more detail, we extracted and analysed a single representative structure for each system obtained from k-means clustering, with details summarised in Table 2, and snapshots of bound residues in Fig. 2. In the case of the 4Glu parent peptide, all four Glu residues are found to be in monodentate contact with uranyl. The equatorial plane is made up by a water molecule at 2.48 Å. In contrast, all phosphorylated peptides are solely coordinated by Glu and pSer residues, with the equatorial plane made up of three κ1 and one κ2 ligands. It is apparent from Table 2 that there is significant variation in U-L distances, with bidentate ligands in some cases shorter but in others longer than analogous monodentate coordination. As well, in some cases distance to Glu is shorter than that to pSer, particularly for monodentate coordination. We ascribe these effects to the steric demands of different ligands and coordination modes, along with the demands of the peptide backbone, since in isolated complexes and smaller model systems the pattern of monodentate shorter than bidentate, and pSer shorter than Glu was evident [38]. In all but one case, the κ2 ligand is pSer, but in pS16 the Glu3 residue is bound through two O atoms, and both pSer through just one. The significance of this difference is discussed in more detail below.

Secondary structure of the peptide was calculated over the 100 ns trajectory for each peptide. In most cases the only defined element of structure was bends, centred on the Pro4-Gly5 and Pro9-Gly10 motifs. However, pS18 shows more rigidly defined secondary structure, with antiparallel β-strands consisting of pSer1-Glu3 and Glu6-pSer8 joined by Pro-Gly turns, a motif that places all four anionic side-chains in perfect alignment to bind uranyl in equatorial plane and which persists over

Table 2
Denticity and U—O distances of representative clusters (Å). κ1 and κ2 refer to mono- and bi-dentate coordination to U, respectively.

	1	3	6	8
4Glu	κ1 2.47	κ1 2.46	κ1 2.46	κ1 2.48
pS16	κ1 2.63	κ2 2.53/2.54	κ1 2.61	κ1 2.52
pS18	κ1 2.64	κ1 2.44	κ1 2.48	κ2 2.62/2.64
pS38	κ1 2.56	κ1 2.63	κ1 2.66	κ2 2.65/2.69
pS68	κ1 2.48	κ1 2.48	κ2 2.65/2.66	κ1 2.59

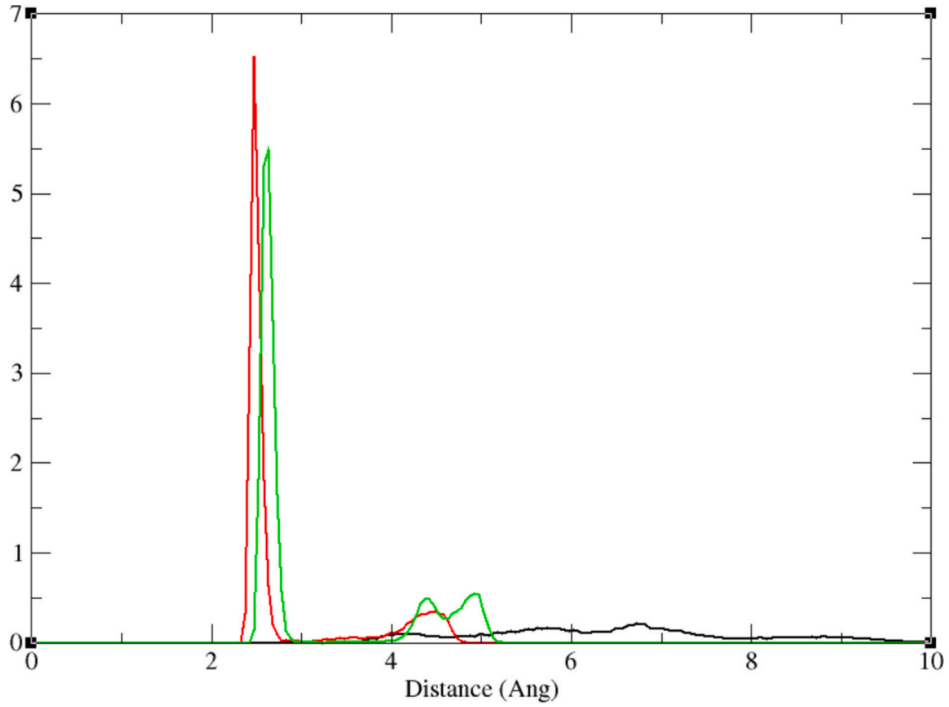

Fig. 1. Radial distribution function (RDF, g(r)) for different O ligands for pS38. pSer shown in green, Glu in red, solvent water in black. (For interpretation of the references to colour in this figure legend, the reader is referred to the web version of this article.)

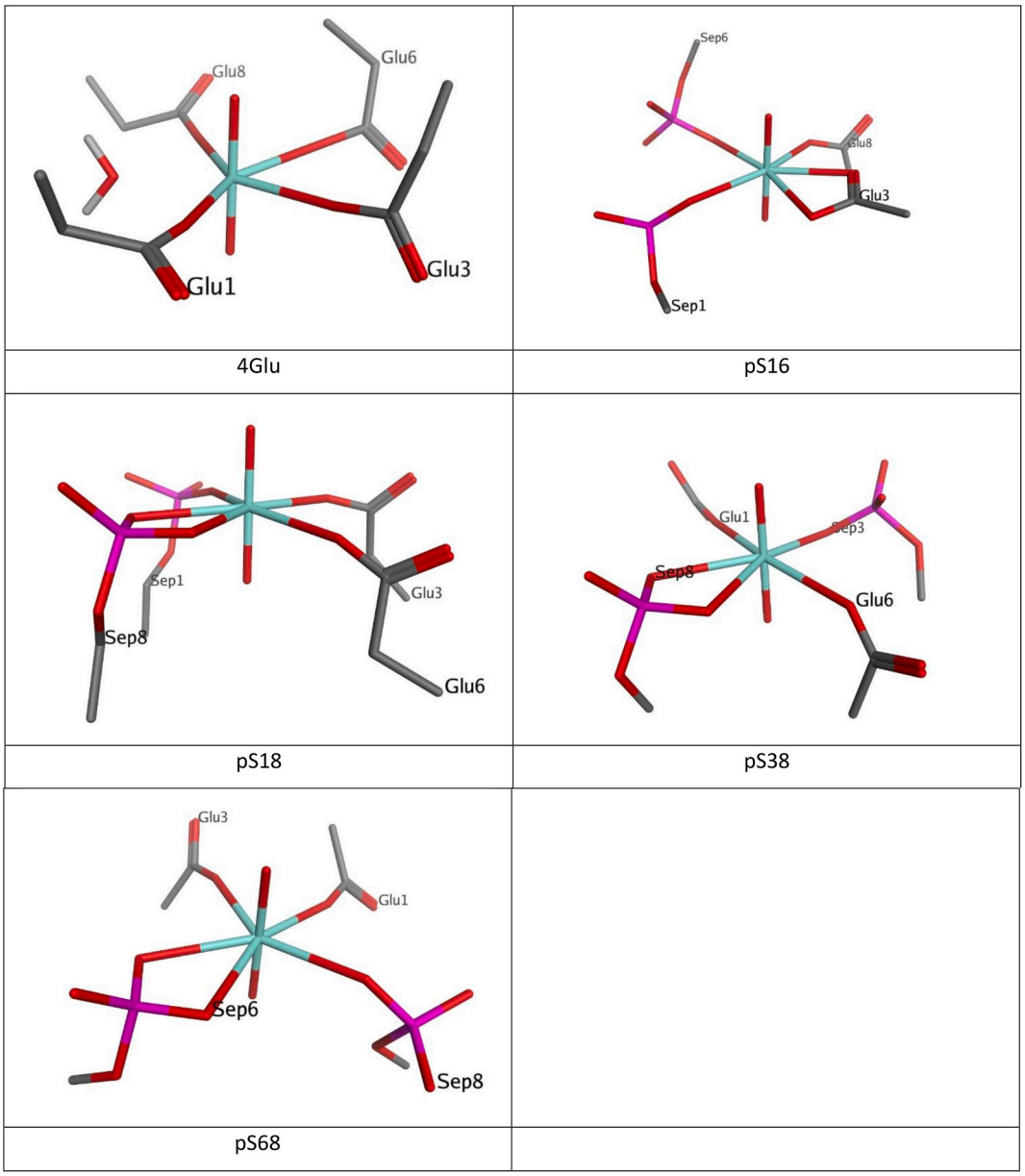

Fig. 2. Detail of first coordination shell for each UO_2^{2+} complex ("Sep" denotes pSer in AMBER PDB files). (For interpretation of the references to colour in this figure legend, the reader is referred to the web version of this article.)

most of the MD trajectory (Fig. 3). For comparison, the geometry of free pS18 is shown (Fig. S4), in which the four coordinating residues are found to lie on the same face of the peptide, but with considerably greater distances from one another than in the bound complex.

The change in backbone structure that results from uranyl binding is evident from the CD spectrum, as shown in Fig. 4. The free peptide shows negative ellipticity at 200 nm, characteristic of an unstructured peptide, whereas the bound peptide exhibits a positive peak at this wavelength and negative ellipticity around 220 nm, exemplifying a structure dominated by β-strands. Thus, it is clear that uranyl binding in this case induces larger changes than just anionic side-chains drawing closer together, allowing the pre-organised structure of the peptide to fully develop. In contrast, all other peptides exhibit CD features typical of unstructured peptides (Fig. S5), indicating that the specific sequence of pS18 is perfectly set up for uranyl binding. These results agree well with experimental data obtained by titration of pS18 with UO_2^{2+} followed by CD, which demonstrates growth of the band distinctive for the β-sheet emergence at 207 nm upon addition of uranyl [20], which is also evidenced at ~200 nm by our computation. The precursor of pS18 (the peptide A1) and the tetraphosphorylated derivative pS1368 both showcase a similar increase in the CD of titration data around 195–200 nm [11] and 200–210 nm [21], respectively.

Binding energy of uranyl to each peptide was calculated using MM-GBSA method, taking snapshots every 50 frames from the 100 ns MD trajectory (Table 3). In all cases, enthalpy of binding is strongly favourable, while entropy disfavours binding, leading to overall binding free energies of between −260 and − 470 kJ mol^{-1}. For the parent 4Glu peptide binding enthalpy is almost −400 kJ mol^{-1}, but phosphorylation enhances this markedly, albeit with striking sequence-dependence on the extent of increased binding. Three peptides increase binding by −70 to −80 kJ mol^{-1}, but pS16 binds uranyl much more strongly, by around −180 kJ mol^{-1} excess over the parent peptide. This increased binding strength stems from enhanced enthalpy since entropy change is much less affected by changes in sequence.

MM-GBSA further allows decomposition of binding into per-residue contributions, as shown in Table S2. This largely matches the geometric

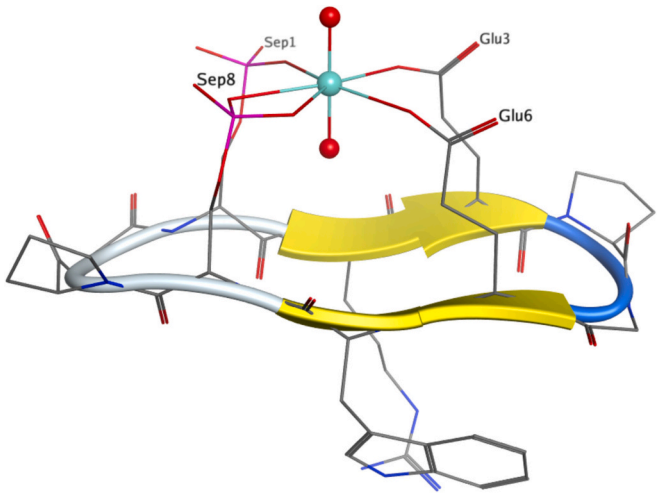

Fig. 3. Secondary structure of pS18-UO_2^{2+} complex: β-strands shown as yellow ribbons, turns as blue tube, heavy atoms shown as wireframe. (For interpretation of the references to colour in this figure legend, the reader is referred to the web version of this article.)

data in Table 2; four Glu residues in the parent 4Glu peptide all contribute strongly to binding, while the remaining six residues are slightly repulsive toward uranyl binding. pSer residues are in general more strongly bound than are Glu, and those that are κ2-bound notably more so than κ1-bound. Again, the exception here is pS16, for which the κ2-bound Glu residue gives the single greatest contribution to binding. This, along with the strong binding from two pSer, seems to be the origin of the anomalous overall binding energy of this peptide. The remaining residues give no more than 10 kJ mol^{-1} to the binding energy, suggesting that outer-shell effects are relatively small in these cases. These data offer some further insight into the particularly strong binding of pS16, for which the single most stabilising residue of all (Glu3) is observed, along with strong binding from all the other anionic residues. Interactions are almost as strong from κ2-bound pSer in other peptides, but these appear to reduce the contribution from the κ1-bound residues.

DFT analysis was performed on the most populated cluster of each system, with solvent and ions stripped out. Geometry optimisation of pS16-UO_2^{2+} gives RMSD between explicit solvent MD and implicit solvent DFT of 1.53 Å for all heavy atoms and 0.85 for UO_2^{2+} and ligands only. This indicates good agreement between MM and DFT data, such that all subsequent analysis is done on single point calculations on MM-minimised geometry. Table 3 reports simple binding energy calculated from DFT data, *i.e.* the electronic energy change for $[UO_2]^{2+}$ + $peptide^{3-}$ ➔ $[UO_2.peptide]^-$ in implicit aqueous solvent. These data confirm the pattern of significantly enhanced binding on incorporation of two pSer residues. Adding entropy correction from MM-GBSA results in overall free energy of binding of a little less than −500 kJ mol^{-1} for 4Glu, and a little over −500 kJ mol^{-1} for phosphorylated peptides. However, in these data the variation between phosphorylated peptides is much smaller than in MM-GBSA (less than 20 kJ mol^{-1}), and here pS18 is predicted to be the strongest binder. Experimental conditions use iminodiacetic acid (IDA) as a competitive binder: at the same level we calculate the binding energy of IDA with uranyl to be −408.4 kJ mol^{-1}, confirming the peptides are significantly better binders than this synthetic ligand.

It is notable that binding energies are significantly larger than experimental data from conditional stability constants in ref. [20] (between 45 and 50 kJ mol^{-1}). Table 3 also reports DFT binding energy derived from the reaction scheme $[UO_2.peptide]^- + 3Cl^- + 2H_2O$ ➔ $[UO_2(Cl)_3(H_2O)_2]^- + peptide^{3-}$, to avoid issues with charge separation that can occur with implicit solvation models. These values are much closer to experimental data for phosphorylated peptides, in the range of 75–80 kJ mol^{-1}, but suggest that the parent 4Glu peptide is a poor binder for uranyl. We note that we are unable to correct these values for entropy, since the peptide complexes are too large for DFT calculation.

Further insight into these trends is drawn from QTAIM analysis, in the form of the electron density at bond critical points ρ_{BCP} for U—O interactions (Table S3). The strong U=O_{yl} interactions are evident in all complexes, the large value of ρ_{BCP} being indicative of significant covalent overlap. Equatorial U—O bonds are also evident, with much lower density values. For the 4Glu complex, κ1-bound Glu residues each have associated BCP with density around 0.05 au, with similar value for bond to water. Each phosphorylated peptide has five BCPs in equatorial plane, matching the geometric analysis from Table 2. ρ_{BCP} for Glu tends to be slightly larger (0.05 au) than that for pSer (0.04 au) but differences are small: an illustration of the molecular graph around U for pS18 is shown in Fig. 5. As well as direct U—O interaction, QTAIM identifies numerous secondary interactions, most notably C-H…O contacts with O_{yl} atoms. However, these are an order of magnitude weaker than the direct interactions, as judged by ρ_{BCP}, suggesting that they are not the origin of observed differences in binding strength. Wiberg bond orders (Table 5)

Table 3
MM-GBSA and DFT binding enthalpy, entropy and free energy (kJ mol^{-1}).

	MM-GBSA			DFT		DFT reaction
	ΔH	TΔS	ΔG	ΔE	ΔG [a]	
4Glu	−418.1	−97.2	−320.8	−592.0	−494.7	−1.7
pS16	−568.0	−102.5	−465.5	−616.4	−513.9	−76.1
pS18	−459.3	−100.2	−359.1	−634.1	−533.9	−80.5
pS38	−475.5	−98.9	−376.6	−611.8	−512.9	−75.5
pS68	−469.0	−97.5	−371.5	−612.2	−514.7	−75.1

[a] Using TΔS from MM-GBSA analysis.

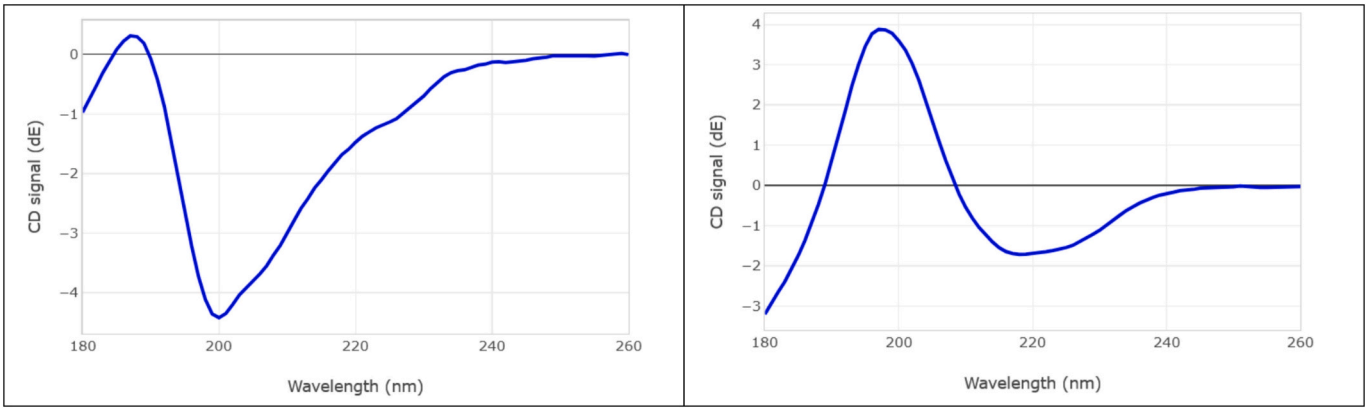

Fig. 4. Predicted CD spectra of a) free and b) uranyl-bound pS18.

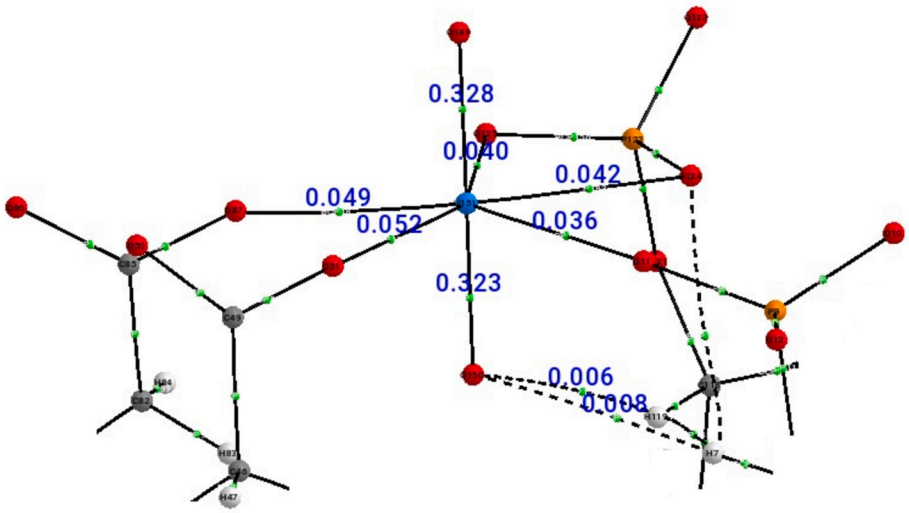

Fig. 5. Molecular graph of pS18-UO_2^{2+} around U. Most atoms not directly involved in uranyl binding are omitted. BCPs are shown as green spheres, bond paths as grey tubes. (For interpretation of the references to colour in this figure legend, the reader is referred to the web version of this article.)

exhibit a similar trend, equatorial ligands' values of 0.4 to 0.6 indicating partial covalency with slightly larger values for bonds to pSer than to Glu.

It is also instructive to note that ρ_{BCP} for U=O_{yl} are significantly lower than those for a model $[UO_2(H_2O)_5]^{2+}$ complex (0.338 au at same theory level). Previous work has shown that competition from equatorial ligands tends to weaken these bonds due to subtle changes in d- and f-orbital energies and occupation. Judged by ρ_{BCP}, the weakest U=O_{yl} bonds are those in pS18, which is also the strongest bound on DFT data. We suggest that these subtle electronic effects, that cannot be easily incorporated into a forcefield description of molecular structure, may be the origin of the discrepancy between MM-GBSA and DFT order of binding energies. We also note that there is, in most cases, some asymmetry in the ρ_{BCP} values for U=O_{yl} bonds: typically, the weaker bond is the one oriented toward the peptide with a greater number of C-H…O_{yl} interactions, as shown in Fig. 5.

Further insight into the electronics of uranyl bonding can be found from Wiberg bond orders, as shown in Table 5. All U=O_{yl} bonds are predicted to have slightly more than a double bond, in agreement with previous studies of model systems [38], and to have little variation in bond order between peptides. All equatorial bonds have order 0.4 to 0.6, with some evidence of slightly greater covalency in bonds to Glu than to pSer, indicating the importance of ionic effects in distinguishing between these possible binding residues. The U—OH_2 bond in 4Glu has order 0.40, comparable to those from peptide ligands.

Starck et al. noted that while most peptides formed 1:1 complexes with uranyl [11], pS16 was found to bind two uranyls simultaneously [20]. We therefore designed a further set of steered and conventional MD to probe this behaviour, using pS16 and pS38 as a comparison. A second uranyl ion was placed outside the 1:1 peptide:UO_2^{2+} complex found above, and pushed into proximity using steered MD. For pS16, using several different starting geometries followed by steered MD/annealing, this process located two possible 2:1 complexes. In the first, one uranyl is bound through both pSer residues, along with backbone O of Glu3, while the other uranyl is bound to both Glu residues, along with backbone O of Gly10, as shown in Fig. 6. The other complex located has the first uranyl bound to both pSer residues and Glu8, as well as backbone O of Gly10 and one water molecule, and the second uranyl monodentate bound to pSer6, Glu3 and Glu8 sidechains, and Glu3 backbone. In this complex, both pSer6 and Glu8 act as bridging ligands between uranyls. In both cases, a single water molecule makes up the equatorial coordination. In contrast to pS16, pushing a second uranyl into the 1:1 UO_2^{2+}:pS38 complex does not result in a stable complex, nor does it disrupt the existing coordination sphere. We speculate that the specific binding mode noted above for pS16 facilitates this 2:1 binding since both pSer residues are bound in κ1 fashion, leaving two phosphoryl oxygens free to bind a second uranyl. We note that both 2:1 complexes are relatively unstructured in the peptide backbone, with all residues being assigned as either coil or bend by DSSP. This does not agree with experimental findings, for which a highly organised β-sheet structure was reported [20]; despite extensive sampling of trajectories, we were unable to locate such structures.

DFT calculations on the first 2:1 complex show that the first uranyl, bound to 2 pSer residues, has binding energy −385.2 kJ mol^{-1}, while the second (Glu bound) uranyl has binding energy of −293.9 kJ mol^{-1}. These are markedly less than the values of *ca.* -500 kJ mol^{-1} for 1:1 complexes noted above, presumably reflecting the smaller number of equatorial ligands available for each uranyl. There is also some evidence for cooperativity in binding, as the overall binding energy of two uranyls is approximately 54 kJ mol^{-1} more negative than the sum of individual binding. In comparison, we were unable to converge DFT calculations on the second 2:1 complex, so cannot report binding energies for this. QTAIM analysis of this 2:1 complex shows that one uranyl is κ2-bound to pSer1 (ρ_{BCP} = 0.050, 0.047) and pSer6 (ρ_{BCP} = 0.042, 0.038) along with two backbone O-atoms (ρ_{BCP} = 0.046, 0.042). The other uranyl is bound in κ2-manner to Glu3 (ρ_{BCP} = 0.049, 0.045 au) and Glu8 (ρ_{BCP} = 0.061, 0.055), and also to three peptide O-atoms (ρ_{BCP} = 0.049, 0.045, 0.043). The involvement of the backbone seems to be vital to the ability of this peptide to bind two uranyl moieties since the anionic sidechains alone are insufficient in number and too geometrically restricted to complete the coordination requirements of uranyl.

Table 5
Wiberg bond orders.

	U=O_{yl}	1	3	6	8
4Glu	2.19, 2.20	0.56	0.55	0.55	0.52
pS16	2.14, 2.14	0.46	0.37, 0.39	0.48	0.43
pS18	2.15, 2.15	0.48	0.55	0.53	0.47, 0.46
pS38	2.13, 2.13	0.48	0.44	0.43	0.46, 0.43
pS68	2.18, 2.15	0.50	0.51	0.45, 0.43	0.52

4. Conclusions

We were able to gain mechanistic understanding of uranyl binding by the cyclic peptide 4Glu and its phosphorylated derivatives by means of previously designed cationic dummy atom (CDA) model of UO_2^{2+},

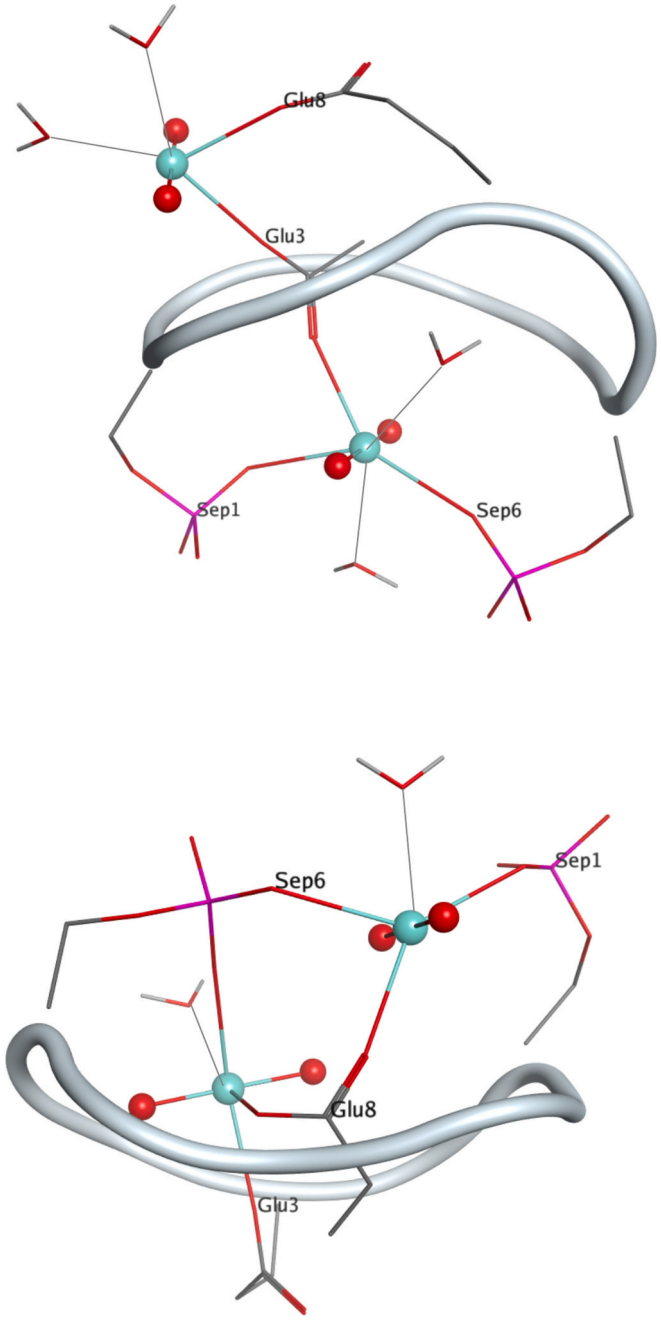

Fig. 6. Two possible structures of 2:1 uranyl:pS16 complex.

combined with well-known forcefields for peptide and water, in MD simulations. The obtained results were confirmed by DFT calculations which produced binding energies and wavefunctions, the analysis of which yields the covalent strength of each separate bond. It also indicates that non-covalent interactions to uranyl oxygen play only a minor role in binding.

Primarily, this investigation has demonstrated that the CDA model of uranyl works well in MD simulations, yielding the geometry very close to the DFT-optimized structure, RMSD between these two methodologies being only 0.85 Å for the uranyl and its first coordination. This shows that the simple CDA model in classical MD simulation enables us to predict the geometry with almost QM-level accuracy. We show the reproducibility of the uranyl binding by the phosphorylated peptides since both the steered MD and annealing produced the almost identical structures. Moreover, use of implicit solvent and enhanced sampling allows rapid and automated identification of bound structures from sequence alone, although subsequent equilibration in explicit water is important for all details of uranyl binding to emerge.

The simulated CD spectra showed the unstructured character of the non-metalated cyclic peptides, which changes drastically upon the binding of uranyl, the presence of which affects the whole decapeptide due to the uranyl holding together the anionic residues. Their binding to the equatorial plane of the uranyl positions their negatively charged oxygens directed toward uranium, such that they no longer strongly affect neighbouring residues, leading to reorganization of the whole peptide. Furthermore, the presented results corroborated the experimental conclusion on the 1:1 complexes formed by these peptides and uranyl. We show that, in most cases, these peptides cannot chelate two uranyls as robustly as a single uranyl since there are insufficient anionic residues to saturate the empty coordination sites of two UO_2^{2+} units. However, the specific arrangement of anionic residues in pS16 allows 2:1 adduct to form, with some evidence of cooperativity of binding obtained from DFT data.

CRediT authorship contribution statement

James A. Platts: Writing – review & editing, Writing – original draft, Visualization, Validation, Methodology, Investigation, Data curation, Conceptualization. **Iogann Tolbatov:** Writing – review & editing, Writing – original draft, Validation, Methodology, Investigation.

Declaration of competing interest

The authors declare that they have no known competing financial interests or personal relationships that could have appeared to influence the work reported in this paper.

James Platts: Conceptualization, Methodology, Investigation, Writing, Visualization

Iogann Tolbatov: Methodology, Investigation, Writing, Visualization

Data availability

Data will be made available on request.

Acknowledgements

This work has been funded by the European Union - Next-Generation EU ("PNRR M4C2-Investimento 1.4- CN00000041"). We acknowledge the CINECA award under the ISCRA initiative, for the availability of high performance computing resources and support. IT gratefully acknowledges the usage of HPC resources from Direction du Numérique – Centre de Calcul de l'Université de Bourgogne (DNUM CCUB).

Appendix A. Supplementary data

Supplementary data to this article, consisting of RMSD plots, U-O radial distribution functions, time evolution of DSSP assignment for pS18-UO2 simulation can be found online at https://doi.org/10.1016/j.jinorgbio.2024.112793.

References

[1] E. Ansoborlo, O. Prat, P. Moisy, C. Den Auwer, P. Guilbaud, M. Carriere, B. Gouget, J. Duffield, D. Doizi, T. Vercouter, C. Moulin, Actinide speciation in relation to biological processes, Biochimie 88 (11) (2006) 1605–1618, https://doi.org/10.1016/j.biochi.2006.06.011.

[2] E. Ansoborlo, B. Amekraz, C. Moulin, V. Moulin, F. Taran, T. Bailly, R. Burgada, M. H. Hengé-Napoli, A. Jeanson, C. Den Auwer, L. Bonin, Review of actinide decorporation with chelating agents, C. R. Chimie 10 (10–11) (2007) 1010–1019, https://doi.org/10.1016/j.crci.2007.01.015.

[3] R.W. Leggett, J.D. Harrison, Fractional absorption of ingested uranium in humans, Health Phys. 68 (4) (1995) 484–498.

[4] L. De Castro, A. Manoury, O. Claude, B. Simoneau, V. Monceau, D. Suhard, C. Elie, V. Magneron, L. Roy, C. Bouvier-Capely, C. Ibanez, Renal toxicity and biokinetics models after repeated uranium instillation, Sci. Rep. 13 (1) (2023) 4111, https://doi.org/10.1038/s41598-023-31073-1.

[5] M. Ma, R. Wang, L. Xu, M. Xu, S. Liu, Emerging health risks and underlying toxicological mechanisms of uranium contamination: lessons from the past two decades, Environ. Int. 145 (2020) 106107, https://doi.org/10.1016/j.envint.2020.106107.

[6] A. Garai, P. Delangle, Recent advances in uranyl binding in proteins thanks to biomimetic peptides, J. Inorg. Biochem. 203 (2020) 110936, https://doi.org/10.1016/j.jinorgbio.2019.110936.

[7] R.G. Pearson, Hard and soft acids and bases, J. Am. Chem. Soc. 85 (22) (1963) 3533–3539.

[8] C. Vidaud, D. Bourgeois, D. Meyer, Bone as target organ for metals: the case of f-elements, Chem. Res. Toxicol. 25 (6) (2012) 1161–1175, https://doi.org/10.1021/tx300064m.

[9] P. Kurttio, H. Komulainen, A. Leino, L. Salonen, A. Auvinen, H. Saha, Bone as a possible target of chemical toxicity of natural uranium in drinking water, Environ. Health Perspect. 113 (1) (2005) 68–72, https://doi.org/10.1289/ehp.7475.

[10] L. Zhou, M. Bosscher, C. Zhang, S. Özçubukçu, L. Zhang, W. Zhang, C.J. Li, J. Liu, M.P. Jensen, L. Lai, C. He, A protein engineered to bind uranyl selectively and with femtomolar affinity, Nat. Chem. 6 (3) (2014) 236–241, https://doi.org/10.1038/nchem.1856.

[11] C. Lebrun, M. Starck, V. Gathu, Y. Chenavier, P. Delangle, Engineering short peptide sequences for uranyl binding, Chem. Eur. J. 20 (50) (2014) 16566–16573, https://doi.org/10.1002/chem.201404546.

[12] J.D. Van Horn, H. Huang, Uranium (VI) bio-coordination chemistry from biochemical, solution and protein structural data, Coord. Chem. Rev. 250 (7–8) (2006) 765–775, https://doi.org/10.1016/j.ccr.2005.09.010.

[13] M. Hémadi, N.T. Ha-Duong, J.M., El Hage Chahine, can uranium be transported by the iron-acquisition pathway? Ur uptake by transferrin, J. Phys. Chem. B 115 (14) (2011) 4206–4215, https://doi.org/10.1021/jp111950c.

[14] Y.W. Lin, Uranyl binding to proteins and structural-functional impacts, Biomolecules 10 (3) (2020) 457, https://doi.org/10.3390/biom10030457.

[15] R. Pardoux, S. Sauge-Merle, D. Lemaire, P. Delangle, L. Guilloreau, J.M. Adriano, C. Berthomieu, Modulating uranium binding affinity in engineered calmodulin EF-hand peptides: effect of phosphorylation, PLoS One 7 (8) (2012) e41922, https://doi.org/10.1371/journal.pone.0041922.

[16] S. Safi, G. Creff, A. Jeanson, L. Qi, C. Basset, J. Roques, P.L. Solari, E. Simoni, C. Vidaud, C. Den Auwer, Osteopontin: a uranium phosphorylated binding-site characterization, Chem. Eur. J. 19 (34) (2013) 11261–11269, https://doi.org/10.1002/chem.201300989.

[17] L. Qi, C. Basset, O. Averseng, E. Quéméneur, A. Hagège, C. Vidaud, Characterization of UO_2^{2+} binding to osteopontin, a highly phosphorylated protein: insights into potential mechanisms of uranyl accumulation in bones, Metallomics 6 (1) (2014) 166–176, https://doi.org/10.1039/c3mt00269a.

[18] J. Sodek, B. Ganss, M.D. McKee, Osteopontin, Crit. Rev. Oral Biol. Med. 11 (3) (2000) 279–303, https://doi.org/10.1177/10454411000110030101.

[19] L.D. Silverman, M. Saadia, J.S. Ishal, N. Tishbi, E. Leiderman, I. Kuyunov, B. Recca, C. Reitblat, R. Viswanathan, Hydroxyapatite growth inhibition by osteopontin hexapeptide sequences, Langmuir 26 (12) (2010) 9899–9904, https://doi.org/10.1021/la100272y.

[20] M. Starck, N. Sisommay, F.A. Laporte, S. Oros, C. Lebrun, P. Delangle, Preorganized peptide scaffolds as mimics of phosphorylated proteins binding sites with a high affinity for uranyl, Inorg. Chem. 54 (23) (2015) 11557–11562, https://doi.org/10.1021/acs.inorgchem.5b02249.

[21] F.A. Laporte, C. Lebrun, C. Vidaud, P. Delangle, Phosphate-rich biomimetic peptides shed light on high-affinity hyperphosphorylated uranyl binding sites in phosphoproteins, Chem. Eur. J. 25 (36) (2019) 8570–8578, https://doi.org/10.1002/chem.201900646.

[22] Z. Cao, K. Balasubramanian, Theoretical studies of $UO_2(OH)(H_2O)_n^+$, $UO_2(OH)_2(H_2O)_n$, $NpO_2(OH)(H_2O)_n$, and $PuO_2(OH)(H_2O)_n^+$ ($n \leq 21$) complexes in aqueous solution, J. Chem. Phys. 131 (16) (2009) 164504, https://doi.org/10.1063/1.3244041.

[23] P. Wåhlin, C. Danilo, V. Vallet, F. Réal, J.P. Flament, U. Wahlgren, An investigation of the accuracy of different DFT functionals on the water exchange reaction in hydrated uranyl (VI) in the ground state and the first excited state, J. Chem. Theory Comput. 4 (4) (2008) 569–577, https://doi.org/10.1021/ct700062x.

[24] M. Sundararajan, A.J. Campbell, I.H. Hillier, Catalytic cycles for the reduction of $[UO_2]^{2+}$ by cytochrome C7 proteins proposed from DFT calculations, J. Phys. Chem. A 112 (19) (2008) 4451–4457, https://doi.org/10.1021/jp800209p.

[25] S.O. Odoh, G.D. Bondarevsky, J. Karpus, Q. Cui, C. He, R. Spezia, L. Gagliardi, UO_2^{2+} uptake by proteins: understanding the binding features of the super uranyl binding protein and design of a protein with higher affinity, J. Am. Chem. Soc. 136 (50) (2014) 17484–17494, https://doi.org/10.1021/ja5087563.

[26] F. Brulfert, S. Safi, A. Jeanson, E. Martinez-Baez, J. Roques, C. Berthomieu, P.-L. Solari, S. Sauge-Merle, E. Simoni, Structural environment and stability of the complexes formed between calmodulin and actinyl ions, Inorg. Chem. 55 (6) (2016) 2728–2736, https://doi.org/10.1021/acs.inorgchem.5b02440.

[27] M.G. Benavides-Garcia, K. Balasubramanian, Structural insights into the binding of uranyl with human serum protein Apotransferrin structure and spectra of protein−uranyl interactions, Chem. Res. Toxicol. 22 (9) (2009) 1613–1621, https://doi.org/10.1021/tx900184r.

[28] M.A. González, Force fields and molecular dynamics simulations, Collection SFN 12 (2011) 169–200, https://doi.org/10.1051/sfn/201112009.

[29] P. Guilbaud, G. Wipff, Hydration of uranyl (UO_2^{2+}) cation and its nitrate ion and 18-crown-6 adducts studied by molecular dynamics simulations, J. Phys. Chem. 97 (21) (1993) 5685–5692, https://doi.org/10.1021/j100123a037.

[30] M. Duvail, T. Dumas, A. Paquet, A. Coste, L. Berthon, P. Guilbaud, UO_2^{2+} structure in solvent extraction phases resolved at molecular and supramolecular scales: a combined molecular dynamics, EXAFS and SWAXS approach, Phys. Chem. Chem. Phys. 21 (15) (2019) 7894–7906, https://doi.org/10.1039/C8CP07230B.

[31] T.-N. Nguyen, M. Duvail, A. Villard, J.J. Molina, P. Guilbaud, J.-F. Dufrêche, Multi-scale modelling of uranyl chloride solutions, J. Chem. Phys. 142 (2) (2015) 024501, https://doi.org/10.1063/1.4905008.

[32] S. Kerisit, C. Liu, Structure, kinetics, and thermodynamics of the aqueous uranyl (VI) cation, J. Phys. Chem. A 117 (30) (2013) 6421–6432, https://doi.org/10.1021/jp404594p.

[33] V. Pomogaev, S.P. Tiwari, N. Rai, G.S. Goff, W. Runde, W.F. Schneider, E.J. Maginn, Development and application of effective pairwise potentials for UO_2^{n+}, NpO_2^{n+}, PuO_2^{n+}, and AmO_2^{n+} (n = 1, 2) ions with water, Phys. Chem. Chem. Phys. 15 (38) (2013), 15954–15963. doi:https://doi.org/10.1039/c3cp52444b.

[34] J.K. Gibson, R.G. Haire, M. Santos, J. Marçalo, A. Pires de Matos, Oxidation studies of dipositive actinide ions, an^{2+} (An = Th, U, np, Pu, am) in the gas phase: synthesis and characterization of the isolated uranyl, neptunyl, and plutonyl ions UO_2^{2+}(g), NpO_2^{2+}(g), and PuO_2^{2+}(g), J. Phys. Chem. A 109 (12) (2005) 2768–2781, https://doi.org/10.1021/jp0447340.

[35] W. Guo, X. Zou, H. Jiang, K.J. Koebke, M. Hoarau, R. Crisci, T. Lu, T. Wei, E.N. G. Marsh, Z. Chen, Molecular structure of the surface-immobilized super uranyl binding protein, J. Phys. Chem. B 125 (28) (2021) 7706–7716, https://doi.org/10.1021/acs.jpcb.1c03849.

[36] S. Sauge-Merle, F. Brulfert, R. Pardoux, P.L. Solari, D. Lemaire, S. Safi, P. Guilbaud, E. Simoni, M.L. Merroun, C. Berthomieu, Structural analysis of uranyl complexation by the EF-hand motif of calmodulin: effect of phosphorylation, Chem. Eur. J. 23 (61) (2017) 15505–15517, https://doi.org/10.1002/chem.201703484.

[37] Y.-W. Lin, C.-M. Nie, L.-F. Liao, Insights into uranyl ion binding to ubiquitin from molecular modeling and dynamics simulations, Chem. Lett. 40 (12) (2011) 1330–1331, https://doi.org/10.1246/cl.2011.1330.

[38] J.A. Platts, I. Tolbatov, Simulation of uranyl-biomolecule interaction using a cationic dummy atom model, Chem. Phys. Lett. 822 (2023) 140479, https://doi.org/10.1016/j.cplett.2023.140479.

[39] D.A. Case, H.M. Aktulga, K. Belfon, D.S. Cerutti, G.A. Cisneros, V.W.D. Cruzeiro, N. Forouzesh, T.J. Giese, A.W. Götz, H. Gohlke, S. Izadi, AmberTools, J. Chem. Inf. Model. 63 (20) (2023) 6183–6191, https://doi.org/10.1021/acs.jcim.3c01153.

[40] J.A. Maier, C. Martinez, K. Kasavajhala, L. Wickstrom, K.E. Hauser, C. Simmerling, ff14SB: improving the accuracy of protein side chain and backbone parameters from ff99SB, J. Chem. Theory Comput. 11 (8) (2015) 3696–3713, https://doi.org/10.1021/acs.jctc.5b00255.

[41] G. Rastelli, A.D. Rio, G. Degliesposti, M. Sgobba, Fast and accurate predictions of binding free energies using MM-PBSA and MM-GBSA, J. Comput. Chem. 31 (4) (2010) 797–810, https://doi.org/10.1002/jcc.21372.

[42] P. Mark, L. Nilsson, Structure and dynamics of the TIP3P, SPC, and SPC/E water models at 298 K, J. Phys. Chem. A 105 (43) (2001) 9954–9960, https://doi.org/10.1021/jp003020w.

[43] V. Kräutler, W.F. Van Gunsteren, P.H. Hünenberger, A fast SHAKE algorithm to solve distance constraint equations for small molecules in molecular dynamics simulations, J. Comput. Chem. 22 (5) (2001) 501–508, https://doi.org/10.1002/1096-987X(20010415)22:5<501::AID-JCC1021>3.0.CO;2-V.

[44] D.R. Roe, T.E. Cheatham III, PTRAJ and CPPTRAJ: software for processing and analysis of molecular dynamics trajectory data, J. Chem. Theory Comput. 9 (7) (2013) 3084–3095, https://doi.org/10.1021/ct400341p.

[45] E.D. Drew, R.W. Janes, PDBMD2CD: providing predicted protein circular dichroism spectra from multiple molecular dynamics-generated protein structures, Nucleic Acids Res. 48 (W1) (2020) W17–W24, https://doi.org/10.1093/nar/gkaa296.

[46] D. Becke, Density-functional thermochemistry. III., The role of exact exchange, J. Chem. Phys. 98 (1993) 5648–5652, https://doi.org/10.1063/1.464913.

[47] W. Lee, R.G. Yang, Parr, development of the Colle-Salvetti correlation-energy formula into a functional of the electron density, Phys. Rev. B 37 (1988) 785, https://doi.org/10.1103/PhysRevB.37.785.

[48] S. Grimme, S. Ehrlich, L. Goerigk, Effect of the damping function in dispersion corrected density functional theory, J. Comput. Chem. 32 (2011) 1456–1465, https://doi.org/10.1002/jcc.21759.

[49] X. Cao, M. Dolg, H. Stoll, Valence basis sets for relativistic energy-consistent small-core actinide pseudopotentials, J. Chem. Phys. 118 (2003) 487–496, https://doi.org/10.1063/1.1521431.

[50] X. Cao, M. Dolg, Segmented contraction scheme for small-core actinide pseudopotential basis sets, J. Mol. Struct. THEOCHEM 673 (2004) 203–209, https://doi.org/10.1016/j.theochem.2003.12.015.

[51] A.D. McLean, G.S. Chandler, Contracted Gaussian basis sets for molecular calculations. I. Second row atoms, Z=11–18, J. Chem. Phys. 72 (1980) 5639–5648, https://doi.org/10.1063/1.438980.

[52] M.M. Francl, W.J. Pietro, W.J. Hehre, J.S. Binkley, M.S. Gordon, D.J. DeFrees, J. A. Pople, Self-consistent molecular orbital methods. XXIII. A polarization-type basis set for second-row elements, J. Chem. Phys. 77 (1982) 3654–3665, https://doi.org/10.1063/1.444267.

[53] J. Tomasi, B. Mennucci, E. Cancès, The IEF version of the PCM solvation method: an overview of a new method addressed to study molecular solutes at the QM ab

initio level, J. Mol. Struct. THEOCHEM 464 (1999) 211–226, https://doi.org/10.1016/S0166-1280(98)00553-3.

[54] M.J. Frisch, G.W. Trucks, H.B. Schlegel, G.E. Scuseria, M.A. Robb, J.R. Cheeseman, G. Scalmani, V. Barone, G.A. Petersson, H. Nakatsuji, et al., Gaussian 16, Revision C.01, Gaussian, Inc., Wallingford, CT, USA, 2016.

[55] T.A. Keith, AIMALL., Version 19.02.13, Gristmill Software, Overland Park KS, USA, 2019.